

A study of time-dependent CP -violating asymmetries in
 $B^0 \rightarrow J/\psi K_s^0$ and $B^0 \rightarrow \psi(2S)K_s^0$ decays

The BABAR Collaboration

July 25, 2000

Abstract

We present a preliminary measurement of time-dependent CP -violating asymmetries in $B^0 \rightarrow J/\psi K_s^0$ and $B^0 \rightarrow \psi(2S)K_s^0$ decays recorded by the BABAR detector at the PEP-II asymmetric-energy B Factory at SLAC. The data sample consists of 9.0 fb^{-1} collected at the $\Upsilon(4S)$ resonance and 0.8 fb^{-1} off-resonance. One of the neutral B mesons, produced in pairs at the $\Upsilon(4S)$, is fully reconstructed. The flavor of the other neutral B meson is tagged at the time of its decay, mainly with the charge of identified leptons and kaons. A neural network tagging algorithm is used to recover events without a clear lepton or kaon tag. The time difference between the decays is determined by measuring the distance between the decay vertices. Wrong-tag probabilities and the time resolution function are measured with samples of fully-reconstructed semileptonic and hadronic neutral B final states. The value of the asymmetry amplitude, $\sin 2\beta$, is determined from a maximum likelihood fit to the time distribution of 120 tagged $B^0 \rightarrow J/\psi K_s^0$ and $B^0 \rightarrow \psi(2S)K_s^0$ candidates to be $\sin 2\beta = 0.12 \pm 0.37$ (stat) ± 0.09 (syst) (preliminary) .

Submitted to the XXXth International Conference on High Energy Physics, Osaka, Japan.

The BABAR Collaboration

B. Aubert, A. Boucham, D. Boutigny, I. De Bonis, J. Favier, J.-M. Gaillard, F. Galeazzi, A. Jeremie,
Y. Karyotakis, J. P. Lees, P. Robbe, V. Tisserand, K. Zachariadou

Lab de Phys. des Particules, F-74941 Annecy-le-Vieux, CEDEX, France

A. Palano

Università di Bari, Dipartimento di Fisica and INFN, I-70126 Bari, Italy

G. P. Chen, J. C. Chen, N. D. Qi, G. Rong, P. Wang, Y. S. Zhu

Institute of High Energy Physics, Beijing 100039, China

G. Eigen, P. L. Reinertsen, B. Stugu

University of Bergen, Inst. of Physics, N-5007 Bergen, Norway

B. Abbott, G. S. Abrams, A. W. Borgland, A. B. Breon, D. N. Brown, J. Button-Shafer, R. N. Cahn,
A. R. Clark, Q. Fan, M. S. Gill, S. J. Gowdy, Y. Groysman, R. G. Jacobsen, R. W. Kadel, J. Kadyk,
L. T. Kerth, S. Kluth, J. F. Kral, C. Leclerc, M. E. Levi, T. Liu, G. Lynch, A. B. Meyer, M. Momayezi,
P. J. Oddone, A. Perazzo, M. Pripstein, N. A. Roe, A. Romosan, M. T. Ronan, V. G. Shelkov, P. Strother,
A. V. Telnov, W. A. Wenzel

Lawrence Berkeley National Lab, Berkeley, CA 94720, USA

P. G. Bright-Thomas, T. J. Champion, C. M. Hawkes, A. Kirk, S. W. O'Neale, A. T. Watson, N. K. Watson

University of Birmingham, Birmingham, B15 2TT, UK

T. Deppermann, H. Koch, J. Krug, M. Kunze, B. Lewandowski, K. Peters, H. Schmuecker, M. Steinke

Ruhr Universität Bochum, Inst. f. Experimentalphysik 1, D-44780 Bochum, Germany

J. C. Andress, N. Chevalier, P. J. Clark, N. Cottingham, N. De Groot, N. Dyce, B. Foster, A. Mass,
J. D. McFall, D. Wallom, F. F. Wilson

University of Bristol, Bristol BS8 1TL, UK

K. Abe, C. Hearty, T. S. Mattison, J. A. McKenna, D. Thiessen

University of British Columbia, Vancouver, BC, Canada V6T 1Z1

B. Camanzi, A. K. McKemey, J. Tinslay

Brunel University, Uxbridge, Middlesex UB8 3PH, UK

V. E. Blinov, A. D. Bukin, D. A. Bukin, A. R. Buzykaev, M. S. Dubrovin, V. B. Golubev,
V. N. Ivanchenko, A. A. Korol, E. A. Kravchenko, A. P. Onuchin, A. A. Salmikov, S. I. Serednyakov,
Yu. I. Skovpen, A. N. Yushkov

*Budker Institute of Nuclear Physics, Siberian Branch of Russian Academy of Science, Novosibirsk 630090,
Russia*

A. J. Lankford, M. Mandelkern, D. P. Stoker

University of California at Irvine, Irvine, CA 92697, USA

A. Ahsan, K. Arisaka, C. Buchanan, S. Chun

University of California at Los Angeles, Los Angeles, CA 90024, USA

J. G. Branson, R. Faccini,¹ D. B. MacFarlane, Sh. Rahatlou, G. Raven, V. Sharma
University of California at San Diego, La Jolla, CA 92093, USA

C. Campagnari, B. Dahmes, P. A. Hart, N. Kuznetsova, S. L. Levy, O. Long, A. Lu, J. D. Richman,
W. Verkerke, M. Witherell, S. Yellin
University of California at Santa Barbara, Santa Barbara, CA 93106, USA

J. Beringer, D. E. Dorfan, A. Eisner, A. Frey, A. A. Grillo, M. Grothe, C. A. Heusch, R. P. Johnson,
W. Kroeger, W. S. Lockman, T. Pulliam, H. Sadrozinski, T. Schalk, R. E. Schmitz, B. A. Schumm,
A. Seiden, M. Turri, D. C. Williams
University of California at Santa Cruz, Institute for Particle Physics, Santa Cruz, CA 95064, USA

E. Chen, G. P. Dubois-Felsmann, A. Dvoretzki, D. G. Hitlin, Yu. G. Kolomensky, S. Metzler, J. Oyang,
F. C. Porter, A. Ryd, A. Samuel, M. Weaver, S. Yang, R. Y. Zhu
California Institute of Technology, Pasadena, CA 91125, USA

R. Aleksan, G. De Domenico, A. de Lesquen, S. Emery, A. Gaidot, S. F. Ganzhur, G. Hamel de
Monchenault, W. Kozanecki, M. Langer, G. W. London, B. Mayer, B. Serfass, G. Vasseur, C. Yeche,
M. Zito
Centre d'Etudes Nucléaires, Saclay, F-91191 Gif-sur-Yvette, France

S. Devmal, T. L. Geld, S. Jayatilleke, S. M. Jayatilleke, G. Mancinelli, B. T. Meadows, M. D. Sokoloff
University of Cincinnati, Cincinnati, OH 45221, USA

J. Blouw, J. L. Harton, M. Krishnamurthy, A. Soffer, W. H. Toki, R. J. Wilson, J. Zhang
Colorado State University, Fort Collins, CO 80523, USA

S. Fahey, W. T. Ford, F. Gaede, D. R. Johnson, A. K. Michael, U. Nauenberg, A. Olivas, H. Park,
P. Rankin, J. Roy, S. Sen, J. G. Smith, D. L. Wagner
University of Colorado, Boulder, CO 80309, USA

T. Brandt, J. Brose, G. Dahlinger, M. Dickopp, R. S. Dubitzky, M. L. Kocian, R. Müller-Pfefferkorn,
K. R. Schubert, R. Schwierz, B. Spaan, L. Wilden
Technische Universität Dresden, Inst. f. Kern- u. Teilchenphysik, D-01062 Dresden, Germany

L. Behr, D. Bernard, G. R. Bonneaud, F. Brochard, J. Cohen-Tanugi, S. Ferrag, E. Roussot, C. Thiebaut,
G. Vasileiadis, M. Verderi
Ecole Polytechnique, Lab de Physique Nucléaire H. E., F-91128 Palaiseau, France

A. Anjomshoaa, R. Bernet, F. Di Lodovico, F. Muheim, S. Playfer, J. E. Swain
University of Edinburgh, Edinburgh EH9 3JZ, UK

C. Bozzi, S. Dittongo, M. Folegani, L. Piemontese
Università di Ferrara, Dipartimento di Fisica and INFN, I-44100 Ferrara, Italy

E. Treadwell
Florida A&M University, Tallahassee, FL 32307, USA

¹ Jointly appointed with Università di Roma La Sapienza, Dipartimento di Fisica and INFN, I-00185 Roma, Italy

R. Baldini-Ferroli, A. Calcaterra, R. de Sangro, D. Falciari, G. Finocchiaro, P. Patteri, I. M. Peruzzi,²
M. Piccolo, A. Zallo

Laboratori Nazionali di Frascati dell'INFN, I-00044 Frascati, Italy

S. Bagnasco, A. Buzzo, R. Contri, G. Crosetti, P. Fabbriatore, S. Farinon, M. Lo Vetere, M. Macri,
M. R. Monge, R. Musenich, R. Parodi, S. Passaggio, F. C. Pastore, C. Patrignani, M. G. Pia, C. Priano,
E. Robutti, A. Santroni

Università di Genova, Dipartimento di Fisica and INFN, I-16146 Genova, Italy

J. Cochran, H. B. Crawley, P.-A. Fischer, J. Lamsa, W. T. Meyer, E. I. Rosenberg
Iowa State University, Ames, IA 50011-3160, USA

R. Bartoldus, T. Dignan, R. Hamilton, U. Mallik
University of Iowa, Iowa City, IA 52242, USA

C. Angelini, G. Batignani, S. Bettarini, M. Bondioli, M. Carpinelli, F. Forti, M. A. Giorgi, A. Lusiani,
M. Morganti, E. Paoloni, M. Rama, G. Rizzo, F. Sandrelli, G. Simi, G. Triggiani

Università di Pisa, Scuola Normale Superiore, and INFN, I-56010 Pisa, Italy

M. Benkebil, G. Grosdidier, C. Hast, A. Hoecker, V. LePeltier, A. M. Lutz, S. Plaszczynski, M. H. Schune,
S. Trincaz-Duvoid, A. Valassi, G. Wormser

LAL, F-91898 ORSAY Cedex, France

R. M. Bionta, V. Brigljević, O. Fackler, D. Fujino, D. J. Lange, M. Mugge, X. Shi, T. J. Wenaus,
D. M. Wright, C. R. Wuest

Lawrence Livermore National Laboratory, Livermore, CA 94550, USA

M. Carroll, J. R. Fry, E. Gabathuler, R. Gamet, M. George, M. Kay, S. McMahon, T. R. McMahon,
D. J. Payne, C. Touramanis

University of Liverpool, Liverpool L69 3BX, UK

M. L. Aspinwall, P. D. Dauncey, I. Eschrich, N. J. W. Gunawardane, R. Martin, J. A. Nash, P. Sanders,
D. Smith

University of London, Imperial College, London, SW7 2BW, UK

D. E. Azzopardi, J. J. Back, P. Dixon, P. F. Harrison, P. B. Vidal, M. I. Williams

University of London, Queen Mary and Westfield College, London, E1 4NS, UK

G. Cowan, M. G. Green, A. Kurup, P. McGrath, I. Scott

University of London, Royal Holloway and Bedford New College, Egham, Surrey TW20 0EX, UK

D. Brown, C. L. Davis, Y. Li, J. Pavlovich, A. Trunov

University of Louisville, Louisville, KY 40292, USA

J. Allison, R. J. Barlow, J. T. Boyd, J. Fullwood, A. Khan, G. D. Lafferty, N. Savvas, E. T. Simopoulos,
R. J. Thompson, J. H. Weatherall

University of Manchester, Manchester M13 9PL, UK

² Jointly appointed with Univ. di Perugia, I-06100 Perugia, Italy

C. Dallapiccola, A. Farbin, A. Jawahery, V. Lillard, J. Olsen, D. A. Roberts
University of Maryland, College Park, MD 20742, USA

B. Brau, R. Cowan, F. Taylor, R. K. Yamamoto
Massachusetts Institute of Technology, Lab for Nuclear Science, Cambridge, MA 02139, USA

G. Blaylock, K. T. Flood, S. S. Hertzbach, R. Kofler, C. S. Lin, S. Willocq, J. Wittlin
University of Massachusetts, Amherst, MA 01003, USA

P. Bloom, D. I. Britton, M. Milek, P. M. Patel, J. Trischuk
McGill University, Montreal, PQ, Canada H3A 2T8

F. Lanni, F. Palombo
Università di Milano, Dipartimento di Fisica and INFN, I-20133 Milano, Italy

J. M. Bauer, M. Booke, L. Cremaldi, R. Kroeger, J. Reidy, D. Sanders, D. J. Summers
University of Mississippi, University, MS 38677, USA

J. F. Arguin, J. P. Martin, J. Y. Nief, R. Seitz, P. Taras, A. Woch, V. Zacek
Université de Montreal, Lab. Rene J. A. Levesque, Montreal, QC, Canada, H3C 3J7

H. Nicholson, C. S. Sutton
Mount Holyoke College, South Hadley, MA 01075, USA

N. Cavallo, G. De Nardo, F. Fabozzi, C. Gatto, L. Lista, D. Piccolo, C. Sciacca
Università di Napoli Federico II, Dipartimento di Scienze Fisiche and INFN, I-80126 Napoli, Italy

M. Falbo
Northern Kentucky University, Highland Heights, KY 41076, USA

J. M. LoSecco
University of Notre Dame, Notre Dame, IN 46556, USA

J. R. G. Alsmiller, T. A. Gabriel, T. Handler
Oak Ridge National Laboratory, Oak Ridge, TN 37831, USA

F. Colecchia, F. Dal Corso, G. Michelon, M. Morandin, M. Posocco, R. Stroili, E. Torassa, C. Voci
Università di Padova, Dipartimento di Fisica and INFN, I-35131 Padova, Italy

M. Benayoun, H. Briand, J. Chauveau, P. David, C. De la Vaissière, L. Del Buono, O. Hamon, F. Le Diberder, Ph. Leruste, J. Lory, F. Martinez-Vidal, L. Roos, J. Stark, S. Versillé
Universités Paris VI et VII, Lab de Physique Nucléaire H. E., F-75252 Paris, Cedex 05, France

P. F. Manfredi, V. Re, V. Speziali
Università di Pavia, Dipartimento di Elettronica and INFN, I-27100 Pavia, Italy

E. D. Frank, L. Gladney, Q. H. Guo, J. H. Panetta
University of Pennsylvania, Philadelphia, PA 19104, USA

M. Haire, D. Judd, K. Paick, L. Turnbull, D. E. Wagoner
Prairie View A&M University, Prairie View, TX 77446, USA

J. Albert, C. Bula, M. H. Kelsey, C. Lu, K. T. McDonald, V. Miftakov, S. F. Schaffner, A. J. S. Smith,
A. Tumanov, E. W. Varnes

Princeton University, Princeton, NJ 08544, USA

G. Cavoto, F. Ferrarotto, F. Ferroni, K. Fratini, E. Lamanna, E. Leonardi, M. A. Mazzoni, S. Morganti,
G. Piredda, F. Safai Tehrani, M. Serra

Università di Roma La Sapienza, Dipartimento di Fisica and INFN, I-00185 Roma, Italy

R. Waldi

Universität Rostock, D-18051 Rostock, Germany

P. F. Jacques, M. Kalelkar, R. J. Plano

Rutgers University, New Brunswick, NJ 08903, USA

T. Adye, U. Egede, B. Franek, N. I. Geddes, G. P. Gopal

Rutherford Appleton Laboratory, Chilton, Didcot, Oxon., OX11 0QX, UK

N. Coptly, M. V. Purohit, F. X. Yumiceva

University of South Carolina, Columbia, SC 29208, USA

I. Adam, P. L. Anthony, F. Anulli, D. Aston, K. Baird, E. Bloom, A. M. Boyarski, F. Bulos, G. Calderini,
M. R. Convery, D. P. Coupal, D. H. Coward, J. Dorfan, M. Doser, W. Dunwoodie, T. Glanzman,
G. L. Godfrey, P. Grosso, J. L. Hewett, T. Himel, M. E. Huffer, W. R. Innes, C. P. Jessop, P. Kim,
U. Langenegger, D. W. G. S. Leith, S. Luitz, V. Luth, H. L. Lynch, G. Manzin, H. Marsiske, S. Menke,
R. Messner, K. C. Moffeit, M. Morii, R. Mount, D. R. Muller, C. P. O'Grady, P. Paolucci, S. Petrak,
H. Quinn, B. N. Ratcliff, S. H. Robertson, L. S. Rochester, A. Roodman, T. Schietinger, R. H. Schindler,
J. Schwiening, G. Sciolla, V. V. Serbo, A. Snyder, A. Soha, S. M. Spanier, A. Stahl, D. Su, M. K. Sullivan,
M. Talby, H. A. Tanaka, J. Va'vra, S. R. Wagner, A. J. R. Weinstein, W. J. Wisniewski, C. C. Young

Stanford Linear Accelerator Center, Stanford, CA 94309, USA

P. R. Burchat, C. H. Cheng, D. Kirkby, T. I. Meyer, C. Roat

Stanford University, Stanford, CA 94305-4060, USA

A. De Silva, R. Henderson

TRIUMF, Vancouver, BC, Canada V6T 2A3

W. Bugg, H. Cohn, E. Hart, A. W. Weidemann

University of Tennessee, Knoxville, TN 37996, USA

T. Benninger, J. M. Izen, I. Kitayama, X. C. Lou, M. Turcotte

University of Texas at Dallas, Richardson, TX 75083, USA

F. Bianchi, M. Bona, B. Di Girolamo, D. Gamba, A. Smol, D. Zanin

Università di Torino, Dipartimento di Fisica Sperimentale and INFN, I-10125 Torino, Italy

L. Bosisio, G. Della Ricca, L. Lanceri, A. Pompili, P. Poropat, M. Prest, E. Vallazza, G. Vuagnin

Università di Trieste, Dipartimento di Fisica and INFN, I-34127 Trieste, Italy

R. S. Panvini

Vanderbilt University, Nashville, TN 37235, USA

C. M. Brown, P. D. Jackson, R. Kowalewski, J. M. Roney
University of Victoria, Victoria, BC, Canada V8W 3P6

H. R. Band, E. Charles, S. Dasu, P. Elmer, J. R. Johnson, J. Nielsen, W. Orejudos, Y. Pan, R. Prepost,
I. J. Scott, J. Walsh, S. L. Wu, Z. Yu, H. Zobernig
University of Wisconsin, Madison, WI 53706, USA

1 Introduction

The CP -violating phase of the three-generation Cabbibo-Kobayashi-Maskawa (CKM) quark mixing matrix can provide an elegant explanation of the well-established CP -violating effects seen in K_L^0 decay [1]. However, studies of CP violation in neutral kaon decays and the resulting experimental constraints on the parameters of the CKM matrix [3] do not in fact provide a test of whether the CKM phase describes CP violation [4].

The unitarity of the three generation CKM matrix can be expressed in geometric form as six triangles of equal area in the complex plane. A nonzero area [5] directly implies the existence of a CP -violating CKM phase. The most experimentally accessible of the unitarity relations, involving the two smallest elements of the CKM matrix, V_{ub} and V_{td} , has come to be known as the Unitarity Triangle. Because the lengths of the sides of the Unitarity Triangle are of the same order, the angles can be large, leading to potentially large CP -violating asymmetries from phases between CKM matrix elements.

The CP -violating asymmetry in $b \rightarrow c\bar{c}s$ decays of the B^0 meson such as $B^0/\bar{B}^0 \rightarrow J/\psi K_s^0$ (or $B^0/\bar{B}^0 \rightarrow \psi(2S)K_s^0$) is caused by the interference between mixed and unmixed decay amplitudes. A state initially prepared as a B^0 (\bar{B}^0) can decay directly to $J/\psi K_s^0$ or can oscillate into a \bar{B}^0 (B^0) and then decay to $J/\psi K_s^0$. With little theoretical uncertainty, the phase difference between these amplitudes is equal to twice the angle $\beta = \arg[-V_{cd}V_{cb}^*/V_{td}V_{tb}^*]$ of the Unitarity Triangle. The CP -violating asymmetry can thus provide a crucial test of the Standard Model. The interference between the two amplitudes, and hence the CP asymmetry, is maximal when the mixing probability is at its highest, *i.e.*, when the lifetime t is approximately 2.2 B^0 proper lifetimes.

In e^+e^- storage rings operating at the $\Upsilon(4S)$ resonance a $B^0\bar{B}^0$ pair produced in $\Upsilon(4S)$ decay evolves in a coherent P -wave until one of the B mesons decays. If one of the B mesons (B_{tag}) can be ascertained to decay to a state of known flavor at a certain time t_{tag} , the other B is *at that time* known to be of the opposite flavor. For this measurement, the other B (B_{CP}) is fully reconstructed in a CP eigenstate ($J/\psi K_s^0$ or $\psi(2S)K_s^0$). By measuring the proper time interval $\Delta t = t_{CP} - t_{tag}$ from the B_{tag} decay time to the decay of the B_{CP} , it is possible to determine the time evolution of the initially pure B^0 or \bar{B}^0 state. The time-dependent rate of decay of the B_{CP} final state is given by

$$f_{\pm}(\Delta t; \Gamma, \Delta m_d, \mathcal{D} \sin 2\beta) = \frac{1}{4} \Gamma e^{-\Gamma|\Delta t|} [1 \pm \mathcal{D} \sin 2\beta \times \sin \Delta m_d \Delta t] , \quad (1)$$

where the $+$ or $-$ sign indicates whether the B_{tag} is tagged as a B^0 or a \bar{B}^0 , respectively. The dilution factor \mathcal{D} is given by $\mathcal{D} = 1 - 2w$, where w is the mistag fraction, *i.e.*, the probability that the flavor of the tagging B is identified incorrectly. A term proportional to $\cos \Delta m_d \Delta t$ would arise from the interference between two decay mechanisms with different weak phases. In the Standard Model, the dominant diagrams (tree and penguin) for the decay modes we consider have no relative weak phase, so no such term is expected.

To account for the finite resolution of the detector, the time-dependent distributions f_{\pm} for B^0 and \bar{B}^0 tagged events (Eq. 1) must be convoluted with a time resolution function $\mathcal{R}(\Delta t; \hat{a})$:

$$\mathcal{F}_{\pm}(\Delta t; \Gamma, \Delta m_d, \mathcal{D} \sin 2\beta, \hat{a}) = f_{\pm}(\Delta t; \Gamma, \Delta m_d, \mathcal{D} \sin 2\beta) \otimes \mathcal{R}(\Delta t; \hat{a}) , \quad (2)$$

where \hat{a} represents the set of parameters that describe the resolution function.

In practice, events are separated into different tagging categories, each of which has a different mean dilution \mathcal{D}_i , determined individually for each category.

It is possible to construct a CP -violating observable

$$\mathcal{A}_{CP}(\Delta t) = \frac{\mathcal{F}_+(\Delta t) - \mathcal{F}_-(\Delta t)}{\mathcal{F}_+(\Delta t) + \mathcal{F}_-(\Delta t)} , \quad (3)$$

which is approximately proportional to $\sin 2\beta$:

$$\mathcal{A}_{CP}(\Delta t) \sim \mathcal{D} \sin 2\beta \times \sin \Delta m_d \Delta t . \quad (4)$$

Since no time-integrated CP asymmetry effect is expected, an analysis of the time-dependent asymmetry is necessary. At an asymmetric-energy B Factory, the proper decay-time difference Δt is, to an excellent approximation, proportional to the distance Δz between the two B^0 -decay vertices along the axis of the boost, $\Delta t \approx \Delta z/c \langle \beta \gamma \rangle$. At PEP-II the average boost of B mesons, $\langle \beta \gamma \rangle$, is 0.56. The distance Δz is $250 \mu\text{m}$ per B^0 lifetime, while the typical Δz resolution for the *BABAR* detector is about $110 \mu\text{m}$.

Since the amplitude of the time-dependent CP -violating asymmetry in Eq. 4 involves the product of \mathcal{D} and $\sin 2\beta$, one needs to determine the dilution factors \mathcal{D}_i (or equivalently the mistag fractions w_i) in order to extract the value of $\sin 2\beta$. The mistag fractions can be extracted from the data by studying the time-dependent rate of $B^0\bar{B}^0$ oscillations in events in which one of the neutral B mesons is fully reconstructed in a self-tagging mode and the other B (the B_{tag}) is flavor-tagged using the standard CP analysis flavor-tagging algorithm. In the limit of perfect determination of the flavor of the fully-reconstructed neutral B , the dilution in the mixed and unmixed amplitudes arises solely from the B_{tag} side, allowing the values of the mistag fractions w_i to be determined.

The value of the single free parameter $\sin 2\beta$ is extracted from the tagged B_{CP} sample by maximizing the likelihood function

$$\ln \mathcal{L}_{CP} = \sum_i \left[\sum_{B^0 \text{ tag}} \ln \mathcal{F}_+(\Delta t; \Gamma, \Delta m_d, \hat{a}, \mathcal{D}_i \sin 2\beta) + \sum_{\bar{B}^0 \text{ tag}} \ln \mathcal{F}_-(\Delta t; \Gamma, \Delta m_d, \hat{a}, \mathcal{D}_i \sin 2\beta) \right] , \quad (5)$$

where the outer summation is over tagging categories i .

1.1 Overview of the analysis

The measurement of the CP -violating asymmetry has five main components :

- Selection of the signal $B^0/\bar{B}^0 \rightarrow J/\psi K_s^0$ and $B^0/\bar{B}^0 \rightarrow \psi(2S)K_s^0$ events, as described in detail in [6].
- Measurement of the distance Δz between the two B^0 decay vertices along the $\mathcal{T}(4S)$ boost axis, as described in detail in [7] and [8].
- Determination of the flavor of the B_{tag} , as described in detail in [7].
- Measurement of the dilution factors \mathcal{D}_i from the data for the different tagging categories, as described in detail in [7].
- Extraction of the amplitude of the CP asymmetry and the value of $\sin 2\beta$ with an unbinned maximum likelihood fit.

Whenever possible, we determine time and mass resolutions, efficiencies and mistag fractions from the data.

2 Sample selection

For this analysis we use a sample of 9.8 fb^{-1} of data recorded by the *BABAR* detector [9] between January 2000 and the beginning of July 2000, of which 0.8 fb^{-1} was recorded 40 MeV below the $\Upsilon(4S)$ resonance (off-resonance data).

A brief description of the *BABAR* detector and the definition of many general analysis procedures can be found in an accompanying paper [9]. Charged particles are detected and their momenta measured by a combination of a central drift chamber (DCH) filled with a helium-based gas and a five-layer, doubled-sided silicon vertex tracker (SVT), in a 1.5 T solenoidal field produced by a superconducting magnet. The charged particle momentum resolution is approximately $(\delta p_T/p_T)^2 = (0.0015 p_T)^2 + (0.005)^2$, where p_T is measured in GeV/ c . The SVT, with typical $10 \mu\text{m}$ single-hit resolution, provides vertex information in both the transverse plane and in the z direction. Vertex resolution is typically $50 \mu\text{m}$ in z for a fully reconstructed B meson, depending on the decay mode, and of order 100 to $150 \mu\text{m}$ for a generic B decay. Leptons and hadrons are identified with measurements from all the *BABAR* components, including the energy loss dE/dx from a truncated mean of up to 40 samples in the DCH and at least 8 samples in the SVT. Electrons and photons are identified in the barrel and the forward regions by the CsI electromagnetic calorimeter (EMC). Muons are identified in the instrumented flux return (IFR). In the central polar region the Cherenkov ring imaging detector (DIRC) provides K - π separation with a significance of at least three standard deviations over the full momentum range for B decay products above $250 \text{ MeV}/c$.

2.1 Particle identification

An electron candidate must be matched to an electromagnetic cluster of at least three crystals in the CsI calorimeter. The ratio of the cluster energy to the track momentum, E/p , must be between 0.88 and 1.3. The lateral moment of the cluster must be between 0.1 and 0.6, and the Zernike moment of order $(4,2)^1$ must be smaller than 0.1. In addition the electron candidate track in the drift chamber must have a dE/dx measurement consistent with that of an electron and, if measured, the Cherenkov angle in the DIRC must be consistent with that of an ultra-relativistic particle.

Muon identification relies principally on the measured number of interaction lengths, N_λ , penetrated by the candidate in the IFR iron, which must have a minimum value of 2.2 and, at higher momenta, must be larger than $N_\lambda^{exp} - 1$, where N_λ^{exp} is the expected number of interaction lengths for a muon. The number of IFR layers with a “hit” must be larger than two. To reject hadronic showers, we impose criteria on the number of IFR strips with a hit as a function of the penetration length, and on the distance between the strips with hits and the extrapolated track. In the forward region, which suffers from accelerator-related background, extra hit-continuity criteria are applied. In addition, if the muon candidate is in the angular region covered by the EMC, the energy deposited by the candidate in the calorimeter must be larger than 50 MeV and smaller than 400 MeV. (The expected energy deposited by a minimum ionizing particle is about 180 MeV.)

Particles are identified as kaons if the ratio of the combined kaon likelihood to the combined pion likelihood is greater than 15. The combined likelihoods are the product of the individual likelihoods in the SVT, DCH and DIRC subsystems. In the SVT and DCH tracking detectors, the likelihoods are based on the measured dE/dx truncated mean compared to the expected mean for the K and π hypotheses, with an assumed Gaussian distribution. The dE/dx resolution is

¹Lateral moment and Zernike moment are cluster shape variables introduced in [9].

estimated on a track-by-track basis, based on the direction and momentum of the track and the number of energy deposition samples. For the DIRC, the likelihood is computed by combining the likelihood of the measured Cherenkov angle compared to the expected Cherenkov angle for a given hypothesis, with the Poisson probability of the number of observed Cherenkov photons, given the number of expected photons for the same hypothesis. DIRC information is not required for particles with momentum less than 0.7 GeV/c, where the DCH dE/dx alone provides good K/π discrimination.

2.2 Data samples

We define three event classes:²

- A CP sample, containing B^0 candidates reconstructed in the CP eigenstates $J/\psi K_S^0$ or $\psi(2S)K_S^0$. The charmonium mesons J/ψ and $\psi(2S)$ are reconstructed through their decays to e^+e^- and $\mu^+\mu^-$. The $\psi(2S)$ is also reconstructed through its decay to $J/\psi\pi^+\pi^-$. The K_S^0 is reconstructed through its decay to $\pi^+\pi^-$ and $\pi^0\pi^0$. The selection criteria for the CP sample are described in the next section.
- Fully reconstructed B^0 samples, containing B^0 candidates in either semileptonic or hadronic flavor eigenstates. The sample of semileptonic decays contains candidates in the $B^0 \rightarrow D^{*-}\ell^+\nu_\ell$ mode ($\ell^+ = e^+$ or μ^+); the sample of hadronic neutral decays contains B^0 candidates in the $D^{(*)-}\pi^+$, $D^{(*)-}\rho^+$ and $D^{(*)-}a_1^+$ modes. A control sample of fully reconstructed B^+ candidates in the $\bar{D}^0\pi^+$ and $\bar{D}^{*0}\pi^+$ (with $\bar{D}^{*0} \rightarrow \pi^0\bar{D}^0$) modes is used for validation studies. The selection criteria for these samples are described in [7] and [8]. We reconstruct ≈ 7500 $B^0 \rightarrow D^{*-}\ell^+\nu_\ell$ candidates, ≈ 2500 candidates in hadronic B^0 final states, and ≈ 2300 candidates in hadronic B^+ final states.
- Charmonium control samples, containing fully reconstructed neutral or charged B candidates in two-body decay modes with a J/ψ in the final state, such as $B^+ \rightarrow J/\psi K^+$ or $B^0 \rightarrow J/\psi K^{*0}(K^{*0} \rightarrow K^+\pi^-)$. The selection criteria for these samples are described in [6]. We reconstruct 570 $B^+ \rightarrow J/\psi K^+$ candidates and 237 $B^0 \rightarrow J/\psi(K^{*0} \rightarrow K^+\pi^-)$ candidates. For the purpose of extracting vertex parameters and mistag rates, the $B^0 \rightarrow J/\psi K^{*0}(K^{*0} \rightarrow K^+\pi^-)$ events are included as part of the fully reconstructed B^0 hadronic sample.

Signal event yields and purities for the individual samples are summarized in Table 1.

2.3 Selection of events in the CP sample

We select events with a minimum of four reconstructed charged tracks in the region defined by $0.41 < \theta_{lab} < 2.41$. Events are required to have a reconstructed vertex within 0.5 cm of the average position of the interaction point in the plane transverse to the beamline, and a total energy greater than 5 GeV in the fiducial regions for charged tracks and neutral clusters. To reduce continuum background, we require the second-order normalized Fox-Wolfram moment[10] ($R_2 = H_2/H_0$) of the event to be less than 0.5.

The selection criteria for the $J/\psi K_S^0$ and $\psi(2S)K_S^0$ events are optimized by maximizing the ratio $\mathcal{S}/\sqrt{\mathcal{S} + \mathcal{B}}$, where \mathcal{S} (the number of signal events that pass the selection) is determined from signal Monte Carlo events, and \mathcal{B} (the number of background events that pass the selection) is

²Throughout this paper, conjugates of flavor-eigenstate modes are implied.

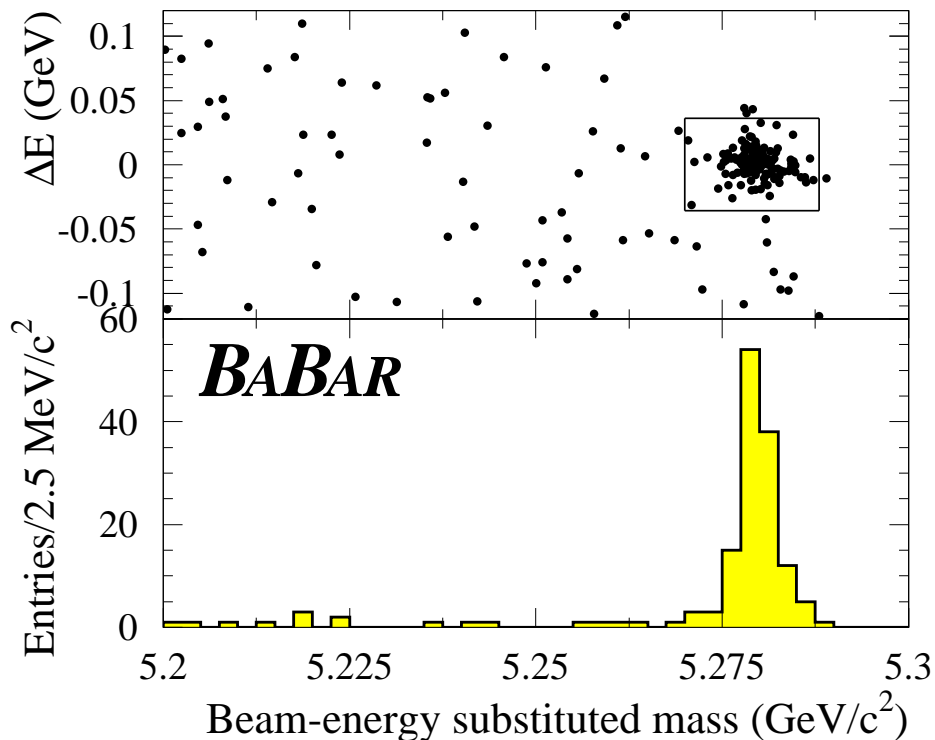


Figure 1: $J/\psi K_S^0$ ($K_S^0 \rightarrow \pi^+\pi^-$) signal.

estimated from a luminosity-weighted average of continuum data events and nonsignal $B\bar{B}$ Monte Carlo events.

For the J/ψ or $\psi(2S) \rightarrow e^+e^-$ candidates, at least one of the decay products is required to be positively identified as an electron or, if outside the acceptance of the calorimeter, to be consistent with an electron according to the drift chamber dE/dx information. If both tracks are within the calorimeter acceptance and have a value of E/p larger than 0.5, an algorithm for the recovery of Bremsstrahlung photons [6] is used.

For the J/ψ or $\psi(2S) \rightarrow \mu^+\mu^-$ candidates, at least one of the decay products is required to be positively identified as a muon and the other, if within the acceptance of the calorimeter, is required to be consistent with a minimum ionizing particle.

We select J/ψ candidates with an invariant mass greater than $2.95 \text{ GeV}/c^2$ and $3.06 \text{ GeV}/c^2$ for the e^+e^- and $\mu^+\mu^-$ modes, respectively, and smaller than $3.14 \text{ GeV}/c^2$ in both cases. The $\psi(2S)$ candidates in leptonic modes must have a mass within $50 \text{ MeV}/c^2$ of the $\psi(2S)$ mass. The lower bound is relaxed to $250 \text{ MeV}/c^2$ for the e^+e^- mode.

For the $\psi(2S) \rightarrow J/\psi \pi^+\pi^-$ mode, mass-constrained J/ψ candidates are combined with pairs of oppositely charged tracks considered as pions, and $\psi(2S)$ candidates with mass between $3.0 \text{ GeV}/c^2$ and $4.1 \text{ GeV}/c^2$ are retained. The mass difference between the $\psi(2S)$ candidate and the J/ψ candi-

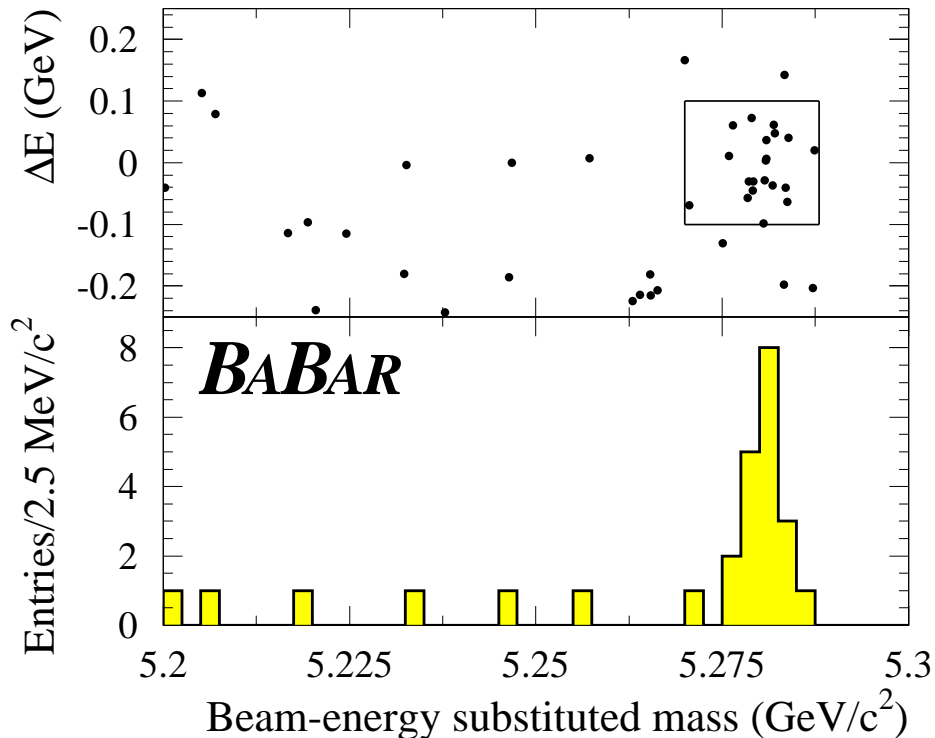


Figure 2: $J/\psi K_s^0$ ($K_s^0 \rightarrow \pi^0\pi^0$) signal.

date is required to be within $15 \text{ MeV}/c^2$ of the known mass difference.

K_s^0 candidates reconstructed in the $\pi^+\pi^-$ mode are required to have an invariant mass, computed at the vertex of the two tracks, between $486 \text{ MeV}/c^2$ and $510 \text{ MeV}/c^2$ for the $J/\psi K_s^0$ selection, and between $491 \text{ MeV}/c^2$ and $505 \text{ MeV}/c^2$ for the $\psi(2S)K_s^0$ selection.

For the $J/\psi K_s^0$ mode, we also consider the decay of the K_s^0 into $\pi^0\pi^0$. Pairs of π^0 candidates, with total energy above 800 MeV and invariant mass, measured at the primary vertex, between 300 and $700 \text{ MeV}/c^2$, are considered as K_s^0 candidates. For each candidate, we determine the most probable K_s^0 decay point along the path defined by the K_s^0 momentum vector and the primary vertex of the event. The decay-point probability is the product of the χ^2 probabilities for each photon pair constrained to the π^0 mass. We require the distance from the decay point to the primary vertex to be between -10 cm and $+40 \text{ cm}$ and the K_s^0 mass measured at this point to be between 470 and $536 \text{ MeV}/c^2$.

B_{CP} candidates are formed by combining mass-constrained J/ψ or $\psi(2S)$ candidates with mass-constrained K_s^0 candidates. The cosine of the angle between the K_s^0 three-momentum vector and the vector that links the J/ψ and K_s^0 vertices must be positive. The cosine of the helicity angle of the J/ψ in the B candidate rest frame must be less than 0.8 for the e^+e^- mode and 0.9 for the $\mu^+\mu^-$ mode.

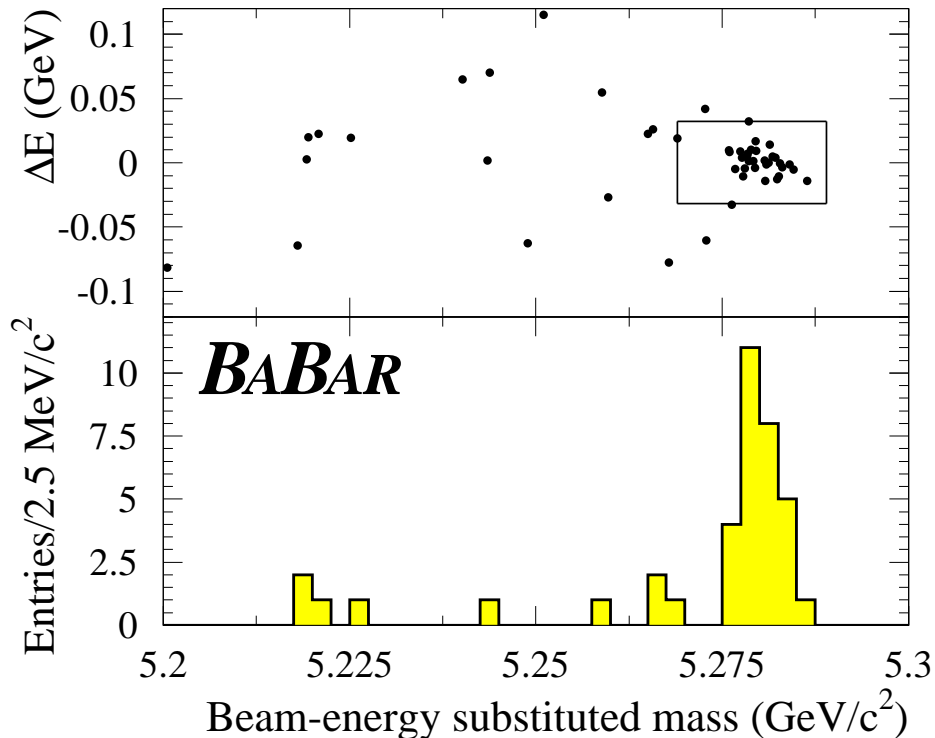


Figure 3: $\psi(2S)K_S^0$ ($K_S^0 \rightarrow \pi^+\pi^-$) signal.

For the $\psi(2S)K_S^0$ candidates, the helicity angle of the $\psi(2S)$ must be smaller than 0.9 for both leptonic modes. The K_S^0 flight length with respect to the $\psi(2S)$ vertex is required to be greater than 1 mm. In the $\psi(2S) \rightarrow J/\psi\pi^+\pi^-$ mode, the absolute value of the cosine of the angle between the B_{CP} candidate three-momentum vector and the thrust vector of the rest of the event, computed in the center-of-mass frame, must be less than 0.9.

B_{CP} candidates are identified with a pair of nearly uncorrelated kinematic variables: the difference ΔE between the energy of the B_{CP} candidate and the beam energy in the center-of-mass frame, and the beam-energy substituted mass m_{ES} [9]. The signal region is defined by $5.270 \text{ GeV}/c^2 < m_{ES} < 5.290 \text{ GeV}/c^2$ and an approximately three-standard-deviation cut on ΔE (typically $|\Delta E| < 35 \text{ MeV}$).

Distributions of ΔE and m_{ES} are shown in Fig. 1, 2 and 3 for the CP samples and in Fig. 4 and 5 for the charmonium control samples. Signal event yields and purities, determined from a fit to the m_{ES} distributions after selection on ΔE , are summarized in Table 1.

The CP sample used in this analysis is composed of 168 candidates: 121 in the $J/\psi K_S^0$ ($K_S^0 \rightarrow \pi^+\pi^-$) channel, 19 in the $J/\psi K_S^0$ ($K_S^0 \rightarrow \pi^0\pi^0$) channel and 28 in the $\psi(2S)K_S^0$ ($K_S^0 \rightarrow \pi^+\pi^-$) channel.

Table 1: Event yields for the different samples used in this analysis, from the fit to m_{ES} distributions after selection on ΔE . The purity is quoted for $m_{ES} > 5.270 \text{ MeV}/c^2$ (except for $D^{*-}\ell^+\nu$).

Sample	Final state	Yield	Purity (%)
CP	$J/\psi K_S^0 (K_S^0 \rightarrow \pi^+\pi^-)$	124 ± 12	96
	$J/\psi K_S^0 (K_S^0 \rightarrow \pi^0\pi^0)$	18 ± 4	91
	$\psi(2S)K_S^0$	27 ± 6	93
Hadronic (neutral)	$D^{*-}\pi^+$	622 ± 27	90
	$D^{*-}\rho^+$	419 ± 25	84
	$D^{*-}a_1^+$	239 ± 19	79
	$D^-\pi^+$	630 ± 26	90
	$D^-\rho^+$	315 ± 20	84
	$D^-a_1^+$	225 ± 20	74
	total	2438 ± 57	85
Hadronic (charged)	$D^0\pi^+$	1755 ± 47	88
	$\bar{D}^*\pi^+$	543 ± 27	89
	total	2293 ± 54	88
Semileptonic	$D^{*-}\ell^+\nu$	7517 ± 104	84
Control	$J/\psi K^+$	597 ± 25	98
	$\psi(2S)K^+$	92 ± 10	93
	$J/\psi K^{*0} (K^{*0} \rightarrow K^+\pi^-)$	251 ± 16	95

3 Time resolution function

The resolution of the Δt measurement is dominated by the z resolution of the tagging vertex. The tagging vertex is determined as follows. The three-momentum of the tagging B and its associated error matrix are derived from the fully reconstructed B_{CP} candidate three momentum, decay vertex and error matrix, and from the knowledge of the average position of the interaction point and the $\Upsilon(4S)$ four-momentum. This derived B_{tag} three-momentum is fit to a common vertex with the remaining tracks in the event (excluding those from B_{CP}). In order to reduce the bias due to long-lived particles, all reconstructed V^0 candidates are used as input to the fit in place of their daughters. Any track whose contribution to the χ^2 is greater than 6 is removed from the fit. This procedure is iterated until there are no tracks contributing more than 6 to the χ^2 or until all tracks are removed. Events are rejected if the fit does not converge for either the B_{CP} or B_{tag} vertex. We also reject events with large Δz ($|\Delta z| > 3 \text{ mm}$) or a large error on Δz ($\sigma_{\Delta z} > 400 \mu\text{m}$).

The time resolution function is described accurately by the sum of two Gaussian distributions, which has five independent parameters:

$$\mathcal{R}(\Delta t; \hat{a}) = \sum_{i=1}^2 \frac{f_i}{\sigma_i \sqrt{2\pi}} \exp\left(-(\Delta t - \delta_i)^2 / 2\sigma_i^2\right). \quad (6)$$

A fit to the time resolution function in Monte Carlo simulated events indicates that most of the events ($f_1 = 1 - f_2 = 70\%$) are in the core Gaussian, which has a width $\sigma_1 \approx 0.6 \text{ ps}$. The wide Gaussian has a width $\sigma_2 \approx 1.8 \text{ ps}$. Tracks from forward-going charm decays included in the reconstruction of the B_{tag} vertex introduce a small bias, $\delta_1 \approx -0.2 \text{ ps}$, for the core Gaussian.

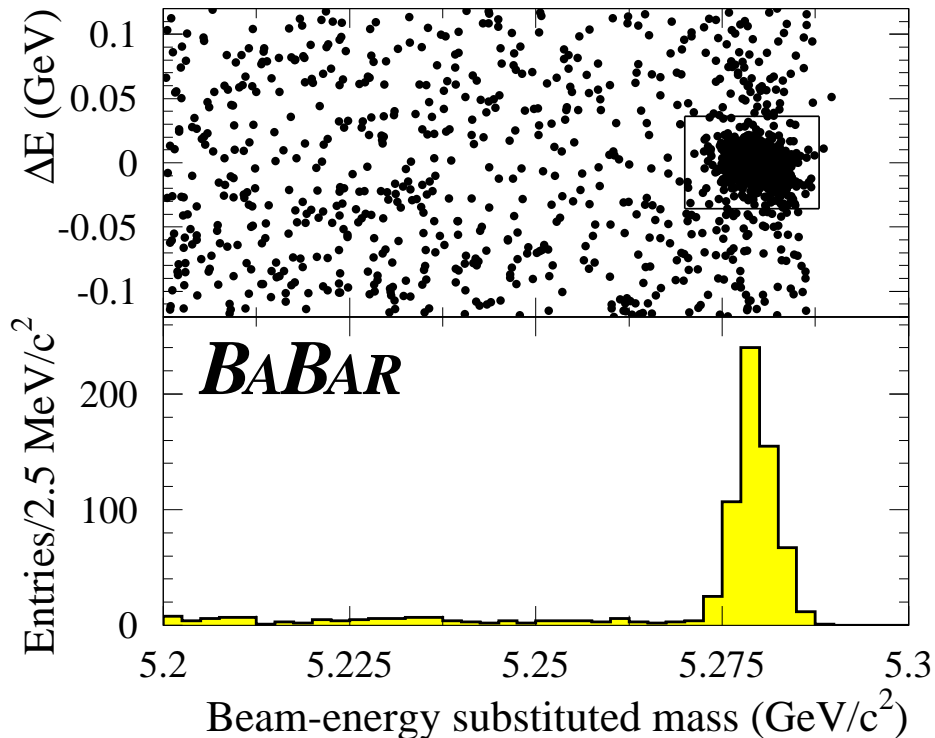


Figure 4: $J/\psi K^+$ signal.

A small fraction of events have very large values of Δz , mostly due to vertex reconstruction problems. This is accounted for in the parametrization of the time resolution function by a very wide unbiased Gaussian with fixed width of 8 ps. The fraction of events populating this component of the resolution function, f_w , is estimated from Monte Carlo simulation as $\sim 1\%$.

In likelihood fits, we use the error $\sigma_{\Delta t}$ on Δt that is calculated from the fits to the two B vertices for each individual event. However, we introduce two scale factors \mathcal{S}_1 and \mathcal{S}_2 for the width of the narrow and the wide Gaussian distributions ($\sigma_1 = \mathcal{S}_1 \times \sigma_{\Delta t}$ and $\sigma_2 = \mathcal{S}_2 \times \sigma_{\Delta t}$) to account for the fact that the uncertainty on Δt is underestimated due to effects such as the inclusion of particles from D decays and possible underestimation of the amount of material traversed by the particles. The scale factor \mathcal{S}_1 and the bias δ_1 of the narrow Gaussian are free parameters in the fit. The scale factor \mathcal{S}_2 and the fraction of events in the wide Gaussian, f_2 , are fixed to the values estimated from Monte Carlo simulation by a fit to the pull distribution ($\mathcal{S}_2 = 2.1$ and $f_2 = 0.25$). The bias of the wide Gaussian, δ_2 , is fixed at 0 ps. The remaining set of three parameters:

$$\hat{a} = \{\mathcal{S}_1, \delta_1, f_w\} \quad (7)$$

is determined from the observed vertex distribution in data.

Because the time resolution is dominated by the precision of the B_{tag} vertex position, we find

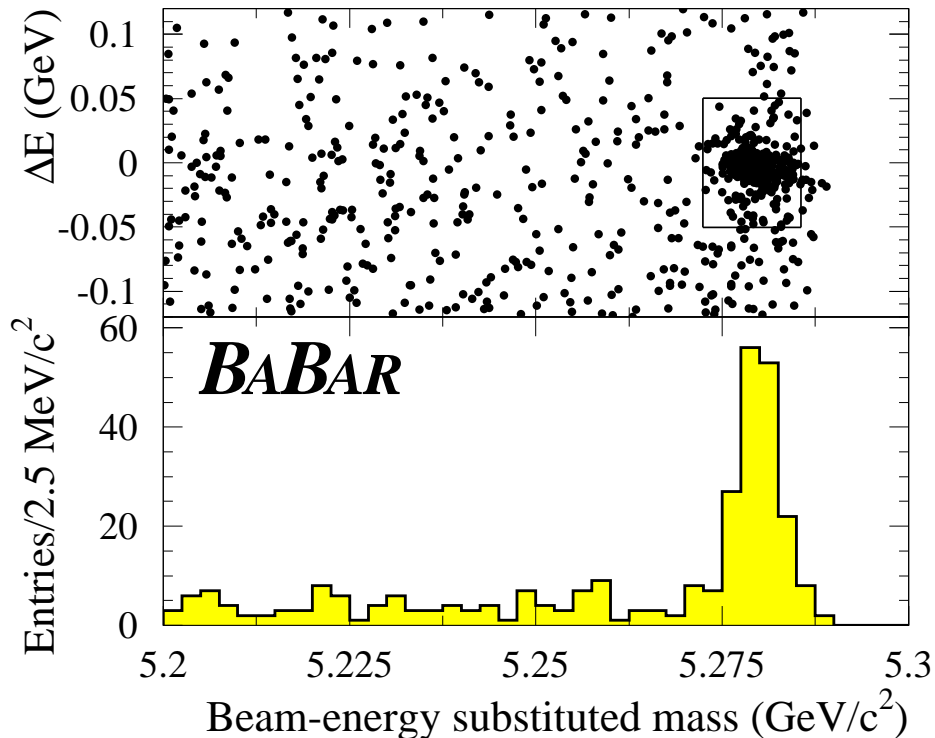


Figure 5: $J/\psi K^{*0}$ ($K^{*0} \rightarrow K^+ \pi^-$) signal.

no significant differences in the Monte Carlo simulation of the resolution function parameters for the various fully reconstructed decay modes, validating our approach of determining the resolution function parameters \hat{a} with the relatively high-statistics fully-reconstructed B^0 data samples. The differences in the resolution function parameters in the different tagging categories are also small.

Table 2 presents the values of the Δt resolution parameters obtained, along with the tagging efficiencies and mistag rates described in Section 4 below, from a maximum likelihood fit to the hadronic B^0 sample. Further details on the procedure and the results can be found in [7]. The vertex parameters are fixed to these values in the final unbinned maximum likelihood fit for $\sin 2\beta$ in the low-statistics CP event sample.

4 B flavor tagging

Each event with a CP candidate is assigned a B^0 or \bar{B}^0 tag if the rest of the event (*i.e.*, with the daughter tracks of the B_{CP} removed) satisfies the criteria for one of several tagging categories. The figure of merit for each tagging category is the effective tagging efficiency $Q_i = \varepsilon_i (1 - 2w_i)^2$, where ε_i is the fraction of events assigned to category i and w_i is the probability of misclassifying the tag

Table 2: Parameters of the resolution function determined from the sample of events with fully-reconstructed hadronic B^0 candidates.

Parameter	Value	
δ_1 (ps)	-0.20 ± 0.06	from fit
\mathcal{S}_1	1.33 ± 0.14	from fit
f_w (%)	1.6 ± 0.6	from fit
f_1 (%)	75	fixed
δ_2 (ps)	0	fixed
\mathcal{S}_2	2.1	fixed

as a B^0 or \bar{B}^0 for this category. w_i is called the mistag fraction. The statistical error on $\sin 2\beta$ is proportional to $1/\sqrt{Q}$, where $Q = \sum_i Q_i$.

Three tagging categories rely on the presence of a fast lepton and/or one or more charged kaons in the event. Two categories, called neural network categories, are based upon the output value of a neural network algorithm applied to events that have not already been assigned to lepton or kaon tagging categories.

In the following, the tag refers to the B_{tag} candidate. In other words, a B^0 tag indicates that the B_{CP} candidate was in a \bar{B}^0 state at $\Delta t = 0$; a \bar{B}^0 tag indicates that the B_{CP} candidate was in a B^0 state.

4.1 Lepton and kaon tagging categories

The three lepton and kaon categories are called **Electron**, **Muon** and **Kaon**. This tagging technique relies on the correlation between the charge of a primary lepton from a semileptonic decay or the charge of a kaon, and the flavor of the decaying b quark. A requirement on the center-of-mass momentum of the lepton reduces contamination from low-momentum opposite-sign leptons coming from charm semileptonic decays. No similar kinematic quantities can be used to discriminate against contamination from opposite-sign kaons. Therefore, for kaons the optimization of Q relies principally on the balance between kaon identification efficiency and the purity of the kaon sample.

The first two categories, **Electron** and **Muon**, require the presence of at least one identified lepton (electron or muon) with a center-of-mass momentum greater than $1.1 \text{ GeV}/c$. The momentum cut rejects the bulk of wrong-sign leptons from charm semileptonic decays. The value is chosen to maximize the effective tagging efficiency Q . The tag is B^0 for a positively-charged lepton, \bar{B}^0 for a negatively-charged lepton.

If the event is not assigned to either the **Electron** or the **Muon** tagging categories, the event is assigned to the **Kaon** tagging category if the sum of the charges of all identified kaons in the event, ΣQ_K , is different from zero. The tag is B^0 if ΣQ_K is positive, \bar{B}^0 otherwise.

If both lepton and kaon tags are present and provide inconsistent flavor tags, the event is rejected from the lepton and kaon tagging categories.

4.2 Neural network categories

The use of a second tagging algorithm is motivated by the potential flavor-tagging power carried by non-identified leptons and kaons, correlations between leptons and kaons, multiple kaons, softer

leptons from charm semileptonic decays, soft pions from D^* decays and more generally by the momentum spectrum of charged particles from B meson decays. One way to exploit the information contained in a set of correlated quantities is to use multivariate methods such as neural networks.

We define five different neural networks, called feature nets, each with a specific goal. Four of the five feature nets are track-based : the L and LS feature nets are sensitive to the presence of primary and cascade leptons, respectively, the K feature net to that of charged kaons and the SoftPi feature net to that of soft pions from D^* decays. In addition, the Q feature net exploits the charge of the fastest particles in the event.

The variables used as input to the neural network tagger are the highest values of the L, LS and SoftPi feature net outputs multiplied by the charge, the highest and the second highest value of the K feature net output multiplied by the charge, and the output of the Q feature net.

The output of the neural network tagger, x_{NT} , can be mapped onto the interval $[-1, 1]$. The tag is B^0 if x_{NT} is negative, \bar{B}^0 otherwise. Events with $|x_{NT}| > 0.5$ are classified in the NT1 tagging category and events with $0.2 < |x_{NT}| < 0.5$ in the NT2 tagging category. Events with $|x_{NT}| < 0.2$ have very little tagging power and are excluded from the sample used in the analysis.

5 Measurement of mistag fractions

The mistag fractions are measured directly in events in which one B^0 candidate, called the B_{rec} , is fully reconstructed in a flavor eigenstate mode. The flavor-tagging algorithms described in the previous section are applied to the rest of the event, which constitutes the potential B_{tag} .

Considering the $B^0\bar{B}^0$ system as a whole, one can classify the tagged events as *mixed* or *unmixed* depending on whether the B_{tag} is tagged with the same flavor as the B_{rec} or with the opposite flavor. Neglecting the effect of possible background contributions, and assuming the B_{rec} is properly tagged, one can express the measured time-integrated fraction of mixed events χ as a function of the precisely-measured $B^0\bar{B}^0$ mixing probability χ_d :

$$\chi = \chi_d + (1 - 2\chi_d)w \quad (8)$$

where $\chi_d = \frac{1}{2} x_d^2 / (1 + x_d^2)$, with $x_d = \Delta m_d / \Gamma$. Thus one can deduce an experimental value of the mistag fraction w from the data.

A time-dependent analysis of the fraction of mixed events is even more sensitive to the mistag fraction. The mixing probability is smallest for small values of $\Delta t = t_{rec} - t_{tag}$ so that the apparent rate of mixed events near $\Delta t=0$ is governed by the mistag probability (see Fig. 6). A time-dependent analysis can also help discriminate against backgrounds with different time-dependence.

By analogy with Eq. 2, we can express the density functions for unmixed (+) and mixed (-) events as

$$\mathcal{H}_{\pm}(\Delta t; \Gamma, \Delta m_d, \mathcal{D}, \hat{a}) = h_{\pm}(\Delta t; \Gamma, \Delta m_d, \mathcal{D}) \otimes \mathcal{R}(\Delta t; \hat{a}), \quad (9)$$

where

$$h_{\pm}(\Delta t; \Gamma, \Delta m_d, \mathcal{D}) = \frac{1}{4} \Gamma e^{-\Gamma|\Delta t|} [1 \pm \mathcal{D} \times \cos \Delta m_d \Delta t]. \quad (10)$$

These functions are used to build the log-likelihood function for the mixing analysis:

$$\ln \mathcal{L}_M = \sum_i \left[\sum_{\text{unmixed}} \ln \mathcal{H}_+(t; \Gamma, \Delta m_d, \hat{a}, \mathcal{D}_i) + \sum_{\text{mixed}} \ln \mathcal{H}_-(t; \Gamma, \Delta m_d, \hat{a}, \mathcal{D}_i) \right], \quad (11)$$

which is maximized to extract the estimates of the mistag fractions $w_i = \frac{1}{2}(1 - \mathcal{D}_i)$.

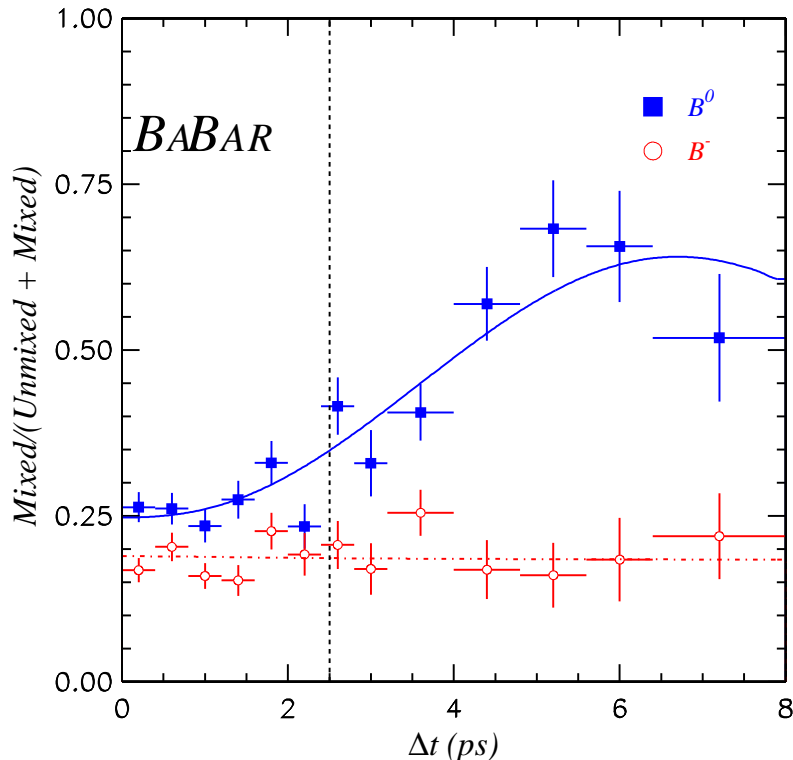


Figure 6: Fraction of mixed events $m/(u + m)$ as a function of $|\Delta t|$ (ps) for data events in the hadronic sample, for neutral B mesons (full squares) and charged B mesons (open circles). All tagging categories are included. This rate is a constant as a function of Δt for charged B mesons, but develops a mixing oscillation for neutral B mesons. The rate of mixed events extrapolated to $\Delta t = 0$ is governed by the mistag fraction w . The dot-dashed line at $t_{cut} = 2.5$ ps indicates the bin boundary of the time-integrated single-bin method.

The extraction of the mistag probabilities for each tagging category is complicated by the possible presence of mode-dependent backgrounds. We deal with these by adding specific terms in the likelihood functions describing the different types of backgrounds (zero lifetime, non-zero lifetime without mixing, non-zero lifetime with mixing). Details are described in [7].

A simple time-integrated single-bin method is used as a check of the time-dependent analysis for the determination of dilutions from the fully reconstructed B^0 sample. The mistag fractions are deduced from the number of unmixed events, u , and the number of mixed events, m , in a single optimized Δt interval, $|\Delta t| < t_{cut}$. The bin boundary t_{cut} , chosen to minimize the statistical uncertainty on the measurement, is equal to 2.5 ps, *i.e.*, 1.6 B^0 lifetimes. (t_{cut} is indicated by a dot-dashed line in Fig. 6.) The resulting mistag fractions based on this method are in good agreement with the mistag fractions obtained with the maximum-likelihood fit [7].

Table 3: Mistag fractions measured from a maximum-likelihood fit to the time distribution for the fully-reconstructed B^0 sample. The **Electron** and **Muon** categories are grouped into one **Lepton** category. The uncertainties on ε and Q are statistical only.

Tagging Category	ε (%)	w (%)	Q (%)
Lepton	11.2 ± 0.5	$9.6 \pm 1.7 \pm 1.3$	7.3 ± 0.3
Kaon	36.7 ± 0.9	$19.7 \pm 1.3 \pm 1.1$	13.5 ± 0.3
NT1	11.7 ± 0.5	$16.7 \pm 2.2 \pm 2.0$	5.2 ± 0.2
NT2	16.6 ± 0.6	$33.1 \pm 2.1 \pm 2.1$	1.9 ± 0.1
all	76.7 ± 0.5		27.9 ± 0.5

5.1 Tagging efficiencies and mistag fractions

The mistag fractions and the tagging efficiencies obtained by combining the results from maximum likelihood fits to the time distributions in the B^0 hadronic and semileptonic samples are summarized in Table 3. We find a tagging efficiency of $(76.7 \pm 0.5)\%$ (statistical error only). The lepton categories have the lowest mistag fractions, but also have low efficiency. The **Kaon** category, despite having a larger mistag fraction (19.7%), has a higher effective tagging efficiency; one-third of events are assigned to this category. Altogether, lepton and kaon categories have an effective tagging efficiency $Q \sim 20.8\%$. Most of the separation into B^0 and \bar{B}^0 in the **NT1** and **NT2** tagging categories derives from the **SoftPi** and **Q** feature nets. Simulation studies indicate that roughly 40% of the effective tagging efficiency occurs in events that contain a soft π aligned with the B_{tag} thrust axis, 25% from events which have a track with $p^* > 1.1 \text{ GeV}/c$, 10% from events which contain multiple leptons or kaons with opposite charges and are thus not previously used in tagging, and the remaining 25% from a mixture of the various feature nets. The neural network categories increase the effective tagging efficiency by $\sim 7\%$ to an overall $Q = (27.9 \pm 0.5)\%$ (statistical error only).

Table 4: Categories of tagged events in the CP sample.

Tagging Category	$J/\psi K_s^0$						$\psi(2S)K_s^0$			CP sample		
	$(K_s^0 \rightarrow \pi^+\pi^-)$			$(K_s^0 \rightarrow \pi^0\pi^0)$			$(K_s^0 \rightarrow \pi^+\pi^-)$			(tagged)		
	B^0	\bar{B}^0	all	B^0	\bar{B}^0	all	B^0	\bar{B}^0	all	B^0	\bar{B}^0	all
Electron	1	3	4	1	0	1	1	2	3	3	5	8
Muon	1	3	4	0	0	0	2	0	2	3	3	6
Kaon	29	18	47	2	2	4	5	7	12	36	27	63
NT1	9	2	11	1	0	1	2	0	2	12	2	14
NT2	10	9	19	3	3	6	3	1	4	16	13	29
Total	50	35	85	7	5	12	13	10	23	70	50	120

Of the 168 CP candidates, 120 are tagged: 70 as B^0 and 50 as \bar{B}^0 . The number of tagged events per category is given in Table 4.

6 Extracting $\sin 2\beta$

6.1 Systematic uncertainties and cross checks

Systematic errors arise from uncertainties in input parameters to the maximum likelihood fit, incomplete knowledge of the time resolution function, uncertainties in the mistag fractions, and possible limitations in the analysis procedure. We fix the B^0 lifetime to the nominal PDG [11] central value $\tau_{B^0} = 1.548$ ps and the value of Δm_d to the nominal PDG value $\Delta m_d = 0.472 \hbar \text{ps}^{-1}$. The errors on $\sin 2\beta$ due to uncertainties in τ_{B^0} and Δm_d are 0.002 and 0.015, respectively. The remaining systematic uncertainties are discussed in the following sections.

6.1.1 Systematic uncertainties in the resolution function

The time resolution is measured with the high-statistics sample of fully-reconstructed B^0 events. The time resolution for the CP sample should be very similar, especially to that measured for the hadronic sample. We verify that the resolution function extracted in the hadronic sample is consistent with the one extracted in the semileptonic sample. We assign as a systematic error the variation in $\sin 2\beta$ obtained by changing the resolution parameters by one statistical standard deviation. The corresponding error on $\sin 2\beta$ is 0.019.

We use a full Monte Carlo simulation to verify that the Bremsstrahlung recovery procedure in the $J/\psi \rightarrow e^+e^-$ mode does not introduce any systematic bias in the Δt measurement, nor does it affect the vertex resolution and pull distributions.

In order to check the impact of imperfect knowledge of the bias in Δt on the measurement, we allow the bias of the second Gaussian to increase to 0.5 ps. The resulting change in $\sin 2\beta$ of 0.047 is assigned as a systematic error. The sensitivity to the bias is due to the different number of events tagged as B^0 and \bar{B}^0 .

6.1.2 Systematic uncertainties in flavor tagging

The mistag fractions are measured with uncertainties that are either correlated or uncorrelated between tagging categories. We study the effect of uncorrelated errors (including statistical errors) on the asymmetry by varying the mistag fractions individually for each category, using the full covariance matrix. For correlated errors, we vary the mistag fractions for all categories simultaneously.

The main common source of systematic uncertainties in the measurement of mistag fractions is the presence of backgrounds, which are more significant in the semileptonic sample than in the hadronic sample. The largest background is due to random combinations of particles and can be studied with mass sidebands. Additional backgrounds arise in the semileptonic sample from misidentified leptons, from leptons incorrectly associated with a true D^* from B decays, and from charm events containing a D^* and a lepton. The details of the procedure for accounting for the backgrounds and the uncertainties on the background levels, and the estimates of resulting systematic errors on the mistag fractions are given in [7]. We estimate the systematic error on $\sin 2\beta$ due to the uncertainties in the measurement of the mistag fractions to be 0.053, for our CP sample.

In the likelihood function, we use the same mistag fractions for the B^0 and \bar{B}^0 samples. However, differences are expected due to effects such as the different cross sections for K^+ and K^- hadronic interactions. For equal numbers of tagged B^0 and \bar{B}^0 events, the impact on $\sin 2\beta$ of a difference in mistag fraction, $\delta w = w_{B^0} - w_{\bar{B}^0}$, is insignificant. From studies of charged and neutral B samples, we

find that the mistag differences are ≤ 0.02 for the NT1 category, ≤ 0.04 for the Kaon category, and negligible for the lepton categories. However, for the NT2 category, there is a significant difference between the B^0 and \bar{B}^0 mistag fractions, $\delta w = 0.16$, which is not predicted by our simulation. Although this would lead to a negligible systematic shift in $\sin 2\beta$, we cover the possibility of different mistag fractions in the CP sample and the fully-reconstructed sample used to measure the mistag fractions by assigning as a systematic uncertainty the shift in $\sin 2\beta$ resulting from using the measured mistag fraction for the NT2 category from the sample of $J/\psi K^{*0}$ events only. The resulting conservative systematic uncertainty on $\sin 2\beta$ is 0.050.

For a small sample of events, there can be a significant difference in the number of B^0 and \bar{B}^0 events, $\Delta N = N_{B^0} - N_{\bar{B}^0}$. For a single tagging category, the fractional change in $\sin 2\beta$ from such a difference is $\Delta \sin 2\beta / \sin 2\beta \approx \delta w \Delta N / N$. In the CP sample, $\Delta N / N$ is significant only in the Kaon and NT1 categories (see Table 4). Taking into account their relative weight in the overall result, we assign a fractional systematic error of 0.005 on $\sin 2\beta$.

The systematic uncertainties on the mistag fractions due to the uncertainties on τ_{B^0} and Δm_d are negligible.

6.1.3 Systematic uncertainties due to backgrounds

The fraction of background events in the CP sample ($J/\psi K_s^0$ and $\psi(2S)K_s^0$) is estimated to be $(5 \pm 3)\%$. The portion of this background that occurs at small values of Δt (*e.g.*, contributions from u , d and s continuum events) does not contribute substantially to the determination of the asymmetry. We estimate that this reduces the effective background to 3%. We correct for the background by increasing the apparent asymmetry by a factor of 1.03. In addition, we assign a fractional systematic uncertainty of 3% on the asymmetry, to cover both the uncertainty in the size of the background and the possibility that the background might have some CP -violating component.

6.1.4 Blind analysis

We have adopted a blind analysis for the extraction of $\sin 2\beta$ in order to eliminate possible experimenter's bias. We use a technique that hides not only the result of the unbinned maximum likelihood fit, but also the visual CP asymmetry in the Δt distribution. The error on the asymmetry is not hidden.

The amplitude of the asymmetry $\mathcal{A}_{CP}(\Delta t)$ from the fit is hidden from the experimenter by arbitrarily flipping its sign and adding an arbitrary offset. The sign flip hides whether a change in the analysis increases or decreases the resulting asymmetry. However, the magnitude of the change is not hidden.

The visual CP asymmetry in the Δt distribution is hidden by multiplying Δt by the sign of the tag and adding an arbitrary offset.

With these techniques, systematic studies can be performed while keeping the numerical value of $\sin 2\beta$ hidden. In particular, we can check that the hidden Δt distributions are consistent for B^0 and \bar{B}^0 tagged events. The same is true for all the other checks concerning tagging, vertex resolution and the correlations between them. For instance, fit results in the different tagging categories can be compared to each other, since each fit is hidden in the same way. The analysis procedure for extracting $\sin 2\beta$ was frozen, and the data sample fixed, prior to unblinding.

Table 5: Result of fitting for CP asymmetries in the entire CP sample and in various subsamples.

sample	$\sin 2\beta$
CP sample	0.12 ± 0.37
$J/\psi K_S^0$ ($K_S^0 \rightarrow \pi^+ \pi^-$) events	-0.10 ± 0.42
other CP events	0.87 ± 0.81
Lepton	1.6 ± 1.0
Kaon	0.14 ± 0.47
NT1	-0.59 ± 0.87
NT2	-0.96 ± 1.30

6.1.5 Cross checks of the fitting procedure

We submitted our maximum-likelihood fitting procedure to an extensive series of simulation tests. The tests were carried out with two different implementations of the fitting algorithm to check for software errors. The validation studies were done on two types of simulated event samples.

- “Toy” Monte Carlo simulation tests. In these samples, the detector response is not simulated. Monte Carlo techniques are used with parametrized resolution functions and tagging probabilities. We validated the fitting procedure on large samples of simulated CP events, for various numbers of tagging categories, values of mistag fractions and values of $\sin 2\beta$. We also simulated a large number of 100-event experiments, with the purpose of investigating statistical issues with small samples, including values of $\sin 2\beta$ near unphysical regions. We checked that the fitter performs well in the presence of backgrounds for the extraction of the mistag fractions. We exercised the combined CP and mixing fits, and found that although combined fits perform well, they do not significantly improve the statistical sensitivity of the result.
- Full Monte Carlo simulation tests. We studied samples of $J/\psi K_S^0$, $J/\psi K^+$, $D^* \pi$ and $D^* \ell \nu$ events produced with the *BABAR* GEANT3 detector simulation and reconstructed with the *BABAR* reconstruction program. $J/\psi K_S^0$ events were generated with various values of $\sin 2\beta$. We extracted the “apparent CP -asymmetry” for the charged B ’s and found it to be consistent with zero. We studied the difference in tagging efficiencies and in mistag fractions between the charged and neutral B samples. We also tested the procedure for extracting the mistag fractions from hadronic and semileptonic samples of fully simulated events ($D^* \pi$ and $D^* \ell \nu$).

6.2 Results

The maximum-likelihood fit for $\sin 2\beta$, using the full tagged sample of $B^0/\bar{B}^0 \rightarrow J/\psi K_S^0$ and $B^0/\bar{B}^0 \rightarrow \psi(2S)K_S^0$ events, gives:

$$\sin 2\beta = 0.12 \pm 0.37 (\text{stat}) \pm 0.09 (\text{syst}) \quad (\text{preliminary}). \quad (12)$$

For this result, the B^0 lifetime and Δm_d are fixed to the current best values [11], and Δt resolution parameters and the mistag rates are fixed to the values obtained from data as summarized in Tables 2 and 3. The log likelihood is shown as a function of $\sin 2\beta$ in Fig. 7, the Δt distributions for B^0 and \bar{B}^0 tags in Fig. 8, the raw asymmetry as a function of Δt in Fig. 9, and the distribution

Table 6: Summary of systematic uncertainties. We compute the fractional systematic errors using the actual value of our asymmetry increased by one statistical standard deviation, that is $0.12 + 0.37 = 0.49$. The different contributions to the systematic error are added in quadrature.

Source of uncertainty	Uncertainty on $\sin 2\beta$
uncertainty on τ_B^0	0.002
uncertainty on Δm_d	0.015
uncertainty on Δz resolution for CP sample	0.019
uncertainty on time-resolution bias for CP sample	0.047
uncertainty on measurement of mistag fractions	0.053
different mistag fractions for CP and non- CP samples	0.050
different mistag fractions for B^0 and \bar{B}^0	0.005
background in CP sample	0.015
total systematic error	0.091

of an observable \mathcal{K} , as a graphical representation of our result, in Fig. 10. The results of the fit for each type of CP sample and for each tagging category are given in Table 5. The contributions to the systematic uncertainty are summarized in Table 6.

We estimate the probability of obtaining the observed value of the statistical uncertainty, 0.37, on our measurement of $\sin 2\beta$ by generating a large number of toy Monte Carlo experiments with

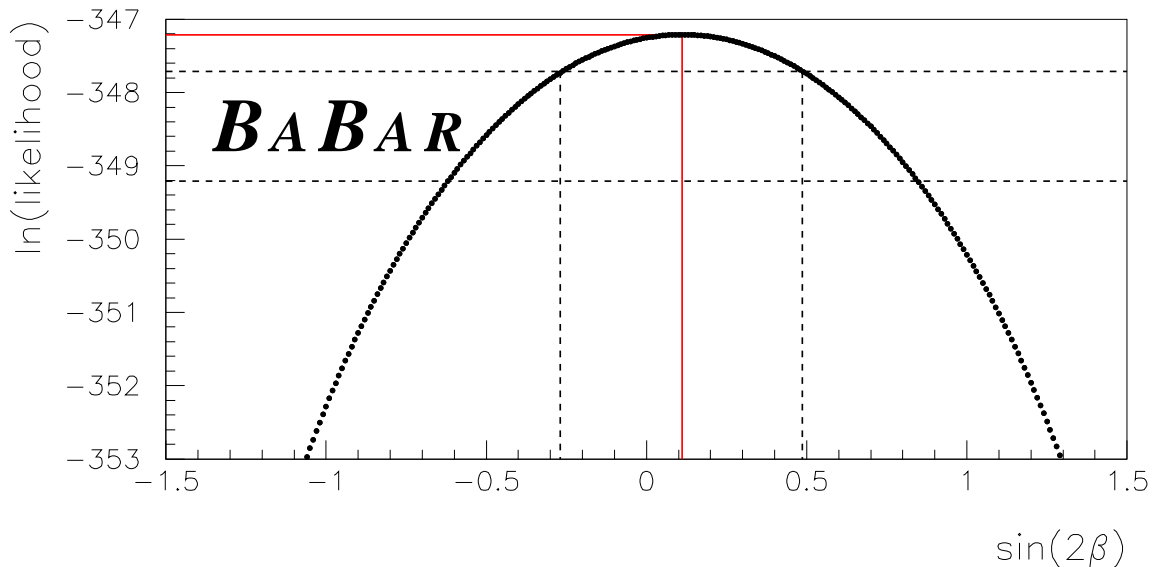


Figure 7: Variation of the log likelihood as a function of $\sin 2\beta$. The two horizontal dashed lines indicate changes in the log likelihood corresponding to one and two statistical standard deviations.

the same number of tagged CP events, and distributed in the same tagging categories, as in the CP sample in the data. We find that the errors are distributed around 0.32 with a standard deviation of 0.03, and that the probability of obtaining a value of the statistical error larger than the one we observe is 5%. Based on a large number of full Monte Carlo simulated experiments with the same number of events as our data sample, we estimate that the probability of finding a lower value of the likelihood than our observed value is 20%.

7 Validating analyses

To validate the analysis we use the charmonium control sample, composed of $B^+ \rightarrow J/\psi K^+$ events and events with self-tagged $J/\psi K^{*0}$ ($K^{*0} \rightarrow K^+ \pi^-$) neutral B 's. We also use the event samples with fully-reconstructed candidates in charged or neutral hadronic modes. These samples should exhibit no time-dependent asymmetry. In order to investigate this experimentally, we define an

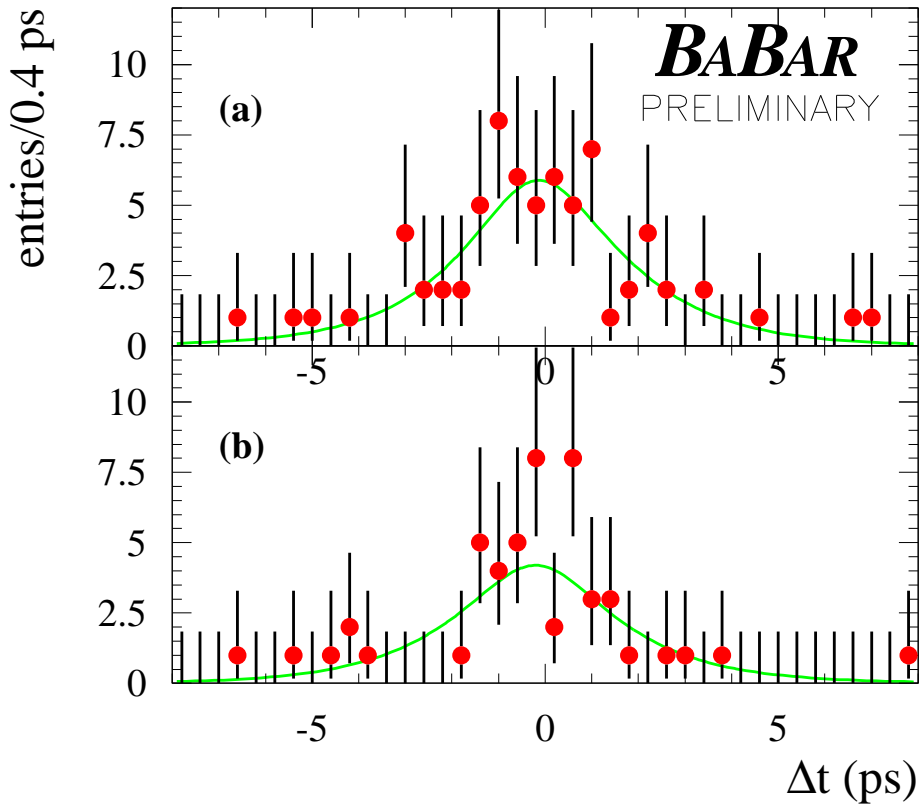


Figure 8: Distribution of Δt for (a) the B^0 tagged events and (b) the \bar{B}^0 tagged events in the CP sample. The error bars plotted for each data point assume Poisson statistics. The curves correspond to the result of the unbinned maximum-likelihood fit and are each normalized to the observed number of tagged B^0 or \bar{B}^0 events.

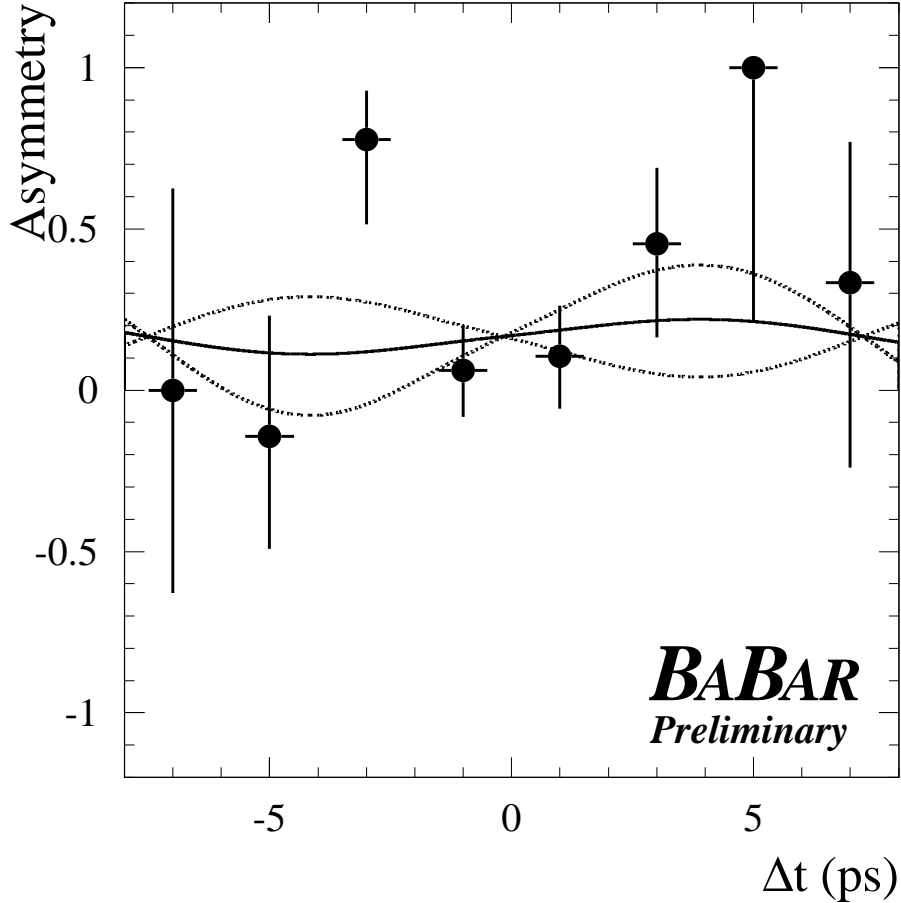


Figure 9: The raw B^0 - \bar{B}^0 asymmetry $(N_{B^0} - N_{\bar{B}^0}) / (N_{B^0} + N_{\bar{B}^0})$, with binomial errors, is shown as a function of Δt . The time-dependent asymmetry is represented by a solid curve for our central value of $\sin 2\beta$, and by two dotted curves for the values at plus and minus one statistical standard deviation from the central value. The curves are not centered at $(0, 0)$ in part because the probability density functions are normalized separately for B^0 and \bar{B}^0 events, and our CP sample contains an unequal number of B^0 and \bar{B}^0 tagged events (70 B^0 versus 50 \bar{B}^0). The χ^2 between the binned asymmetry and the result of the maximum-likelihood fit is 9.2 for 7 degrees of freedom.

“apparent CP asymmetry”, analogous to $\sin 2\beta$ in Eq. 3, which we extract from the data using an identical maximum-likelihood procedure.

The events in the control samples are flavor eigenstates and not CP eigenstates. They are used for testing the fitting procedure with the same tagging algorithm as for the CP sample and, in the case of the B^+ modes, with self-tagging based on their charge. We also perform the fits for B^0 and \bar{B}^0 (or B^+ and B^-) events separately to study possible flavor-dependent systematic effects. For the charged B modes, we use mistag fractions measured from the sample of hadronic charged B decays.

In all fits, including the fits to charged samples, we fix the lifetime τ_{B^0} and the oscillation frequency Δm_d to the PDG values [11]. The results of a series of validation checks on the control samples are summarized in Table 7.

The two high-statistics samples and the $J/\psi K^+$ sample give an apparent CP asymmetry consistent with zero. The 1.9σ asymmetry in the $J/\psi K^{*0}$ is interpreted as a statistical fluctuation.

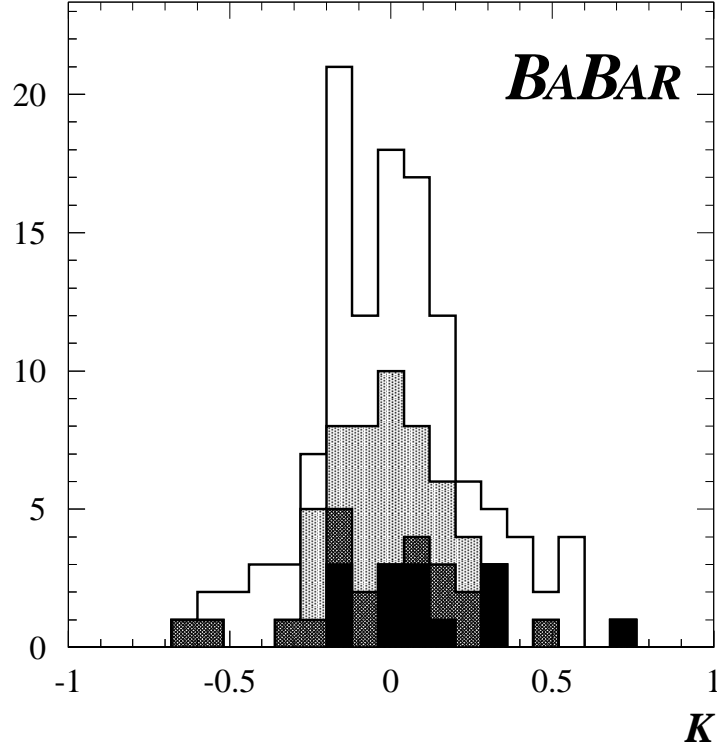


Figure 10: Distribution of $\mathcal{K} = (\varepsilon_{tag}/\sin 2\beta) \times (\mathcal{F}_+ - \mathcal{F}_-) / (\mathcal{F}_+ + \mathcal{F}_-)$, where ε_{tag} is +1 (-1) for a B^0 (\bar{B}^0) tag, respectively (the \mathcal{K} observable would take the simple form $\mathcal{K} = \varepsilon_{tag} \mathcal{D} \sin \Delta m_d \Delta t$ in the ideal case of a perfect time resolution). The value of $\sin 2\beta$ and its statistical error can be derived from the mean value and the 2^{nd} and 4^{th} order momenta of the distribution (see Ref. [2] and [12]) : $\sin 2\beta = \langle \mathcal{K} \rangle / \langle \mathcal{K}^2 \rangle \pm \sqrt{[1 - \sin^2 2\beta \langle \mathcal{K}^4 \rangle / \langle \mathcal{K}^2 \rangle] / [N_{CP} \langle \mathcal{K}^2 \rangle]}$. There are 120 entries in the plot (one per tagged CP event). The contributions of the different tagging categories are indicated: Lepton in black, Kaon in white, NT1 in dark gray, NT2 in light gray. One finds $\langle \mathcal{K} \rangle = 0.0072$, $\langle \mathcal{K}^2 \rangle = 0.062$ and $\langle \mathcal{K}^4 \rangle = 0.013$, yielding $\sin 2\beta = 0.12 \pm 0.37$, which is exactly the result obtained with the maximum-likelihood analysis.

Table 7: Results of fitting for apparent CP asymmetries in various charged or neutral flavor-eigenstate B samples.

Sample	Apparent CP -asymmetry
Hadronic charged B decays	0.03 ± 0.07
Hadronic neutral B decays	-0.01 ± 0.08
$J/\psi K^+$	0.13 ± 0.14
$J/\psi K^{*0}$ ($K^{*0} \rightarrow K^+ \pi^-$)	0.49 ± 0.26

Other *BABAR* time-dependent analyses presented at this Conference demonstrate the validity of the novel technique developed for use at an asymmetric *B* Factory. The measurement of the $B^0\text{-}\bar{B}^0$ oscillation frequency described in [7] uses the same time resolution function and tagging algorithm as the *CP* analysis. Fitting for Δm_d in the maximum-likelihood fit for the fully-reconstructed hadronic and semileptonic neutral *B* decays, we measure

$$\Delta m_d = 0.512 \pm 0.017(\text{stat}) \pm 0.022(\text{syst}) \hbar \text{ps}^{-1} , \quad (13)$$

which is consistent with the world average $\Delta m_d = 0.472 \pm 0.017 \hbar \text{ps}^{-1}$ [11]. The B^0 lifetime measurement described in [8] uses the same inclusive vertex reconstruction technique as the *CP* analysis. We measure

$$\tau_{B^0} = 1.506 \pm 0.052(\text{stat}) \pm 0.029(\text{syst}) \text{ps} , \quad (14)$$

also consistent with the world average $\tau_{B^0} = 1.548 \pm 0.032 \text{ps}$ [11].

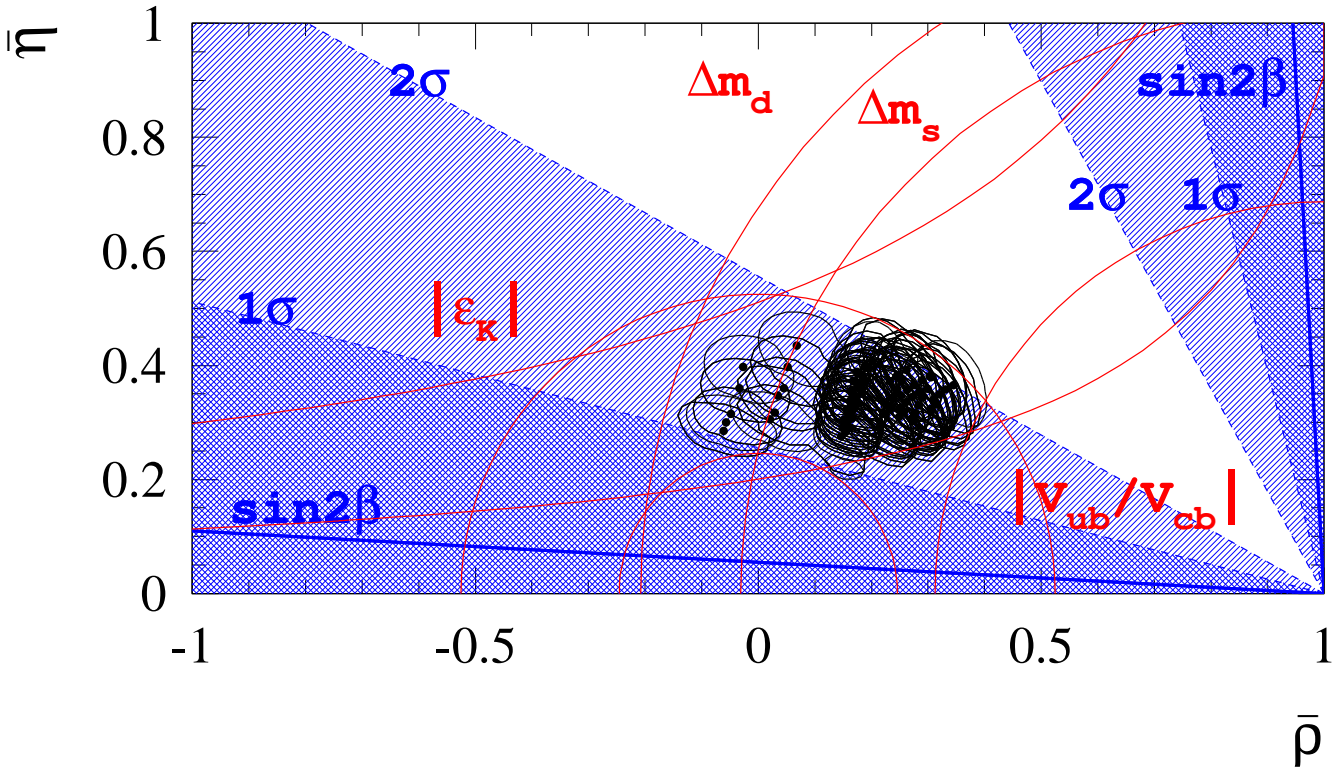


Figure 11: Present constraints on the position of the apex of the Unitarity Triangle in the $(\bar{\rho}, \bar{\eta})$ plane. The fitting procedure is described in Ref [3]. We use the following set of measurements: $|V_{cb}| = 0.0402 \pm 0.017$, $|V_{ub}/V_{cb}| = \langle |V_{ub}/V_{cb}| \rangle \pm 0.0079$, $\Delta m_d = 0.472 \pm 0.017 \hbar \text{ps}^{-1}$ and $|\epsilon_K| = (2.271 \pm 0.017) \times 10^{-3}$, and for Δm_s the set of amplitudes corresponding to a 95%CL limit of $14.6 \hbar \text{ps}^{-1}$. We scan the model-dependent parameters $\langle |V_{ub}/V_{cb}| \rangle$, B_K , $f_{B_d} \sqrt{B_{B_d}}$ and ξ_s , in the range $[0.070, 0.100]$, $[0.720, 0.980]$, $[185, 255] \text{MeV}$ and $[1.07, 1.21]$, respectively. Our result $\sin 2\beta = 0.12 \pm 0.37(\text{stat})$ is represented by cross-hatched regions corresponding to one and two statistical standard deviations.

8 Conclusions and prospects

We have presented *BABAR*'s first measurement of the CP -violating asymmetry parameter $\sin 2\beta$ in the B meson system:

$$\sin 2\beta = 0.12 \pm 0.37 (\text{stat}) \pm 0.09 (\text{syst}) \quad (\text{preliminary}). \quad (15)$$

Our measurement is consistent with the world average $\sin 2\beta = 0.9 \pm 0.4$ [11],³ and is currently limited by the size of the CP sample. We expect to more than double the present data sample in the near future.

Figure 11 shows the Unitarity Triangle in the $(\bar{\rho}, \bar{\eta})$ plane, with *BABAR*'s measured central value of $\sin 2\beta$ shown as two straight lines. There is a two-fold ambiguity in deriving a value of β from a measurement of $\sin 2\beta$. Both choices are shown with cross-hatched regions corresponding to one and two times the one-standard-deviation experimental uncertainty. The ellipses correspond to the regions allowed by all other measurements that constrain the Unitarity Triangle. Rather than make the common, albeit unfounded, assumption that our lack of knowledge of theoretical quantities, or differences between theoretical models, can be parametrized (typically as a Gaussian or flat distribution), we have chosen to display the ellipses corresponding to measurement errors at a variety of representative choices of theoretical parameters. This procedure is discussed in detail in [3].

While the current experimental uncertainty on $\sin 2\beta$ is large, the next few years will bring substantial improvements in precision, as well as measurements for other final states in which CP -violating asymmetries are proportional to $\sin 2\beta$, and measurements for modes in which the asymmetry is proportional to $\sin 2\alpha$.

9 Acknowledgments

We are grateful for the contributions of our PEP-II colleagues in achieving the excellent luminosity and machine conditions that have made this work possible. We acknowledge support from the Natural Sciences and Engineering Research Council (Canada), Institute of High Energy Physics (China), Commissariat à l'Energie Atomique and Institut National de Physique Nucléaire et de Physique des Particules (France), Bundesministerium für Bildung und Forschung (Germany), Istituto Nazionale di Fisica Nucleare (Italy), The Research Council of Norway, Ministry of Science and Technology of the Russian Federation, Particle Physics and Astronomy Research Council (United Kingdom), the Department of Energy (US), and the National Science Foundation (US). In addition, individual support has been received from the Swiss National Foundation, the A. P. Sloan Foundation, the Research Corporation, and the Alexander von Humboldt Foundation. The visiting groups wish to thank SLAC for the support and kind hospitality extended to them.

³Based on the OPAL result [13] $\sin 2\beta = 3.2_{-2.0}^{+1.8} \pm 0.5$ and the CDF result [14] $\sin 2\beta = 0.79_{-0.44}^{+0.41}$. See also ALEPH's preliminary result [15] $\sin 2\beta = 0.93_{-0.88}^{+0.64+0.36} - 0.24$.

References

- [1] J. H. Christenson *et al.*, Phys. Rev. Lett. **13**, 138 (1964);
NA31 Collaboration, G. D. Barr *et al.*, Phys. Lett. **317**, 233 (1993);
E731 Collaboration, L. K. Gibbons *et al.*, Phys. Rev. Lett. **70**, 1203 (1993).
- [2] P. H. Harrison and H. R. Quinn, eds., “The *BABAR* physics book”, SLAC-R-504 (1998).
- [3] See, for instance, “Overall determinations of the CKM matrix”, in [2] section 14 and references therein.
- [4] For an introduction to *CP* violation, see, for instance, “A *CP* violation primer”, in [2] section 1 and references therein.
- [5] C. Jarlskog, in *CP Violation*, C. Jarlskog ed., World Scientific, Singapore (1988).
- [6] *BABAR* Collaboration, B. Aubert *et al.*, “Exclusive *B* decays to charmonium final states”, *BABAR-CONF-00/05*, submitted to the XXXth International Conference on High Energy Physics, Osaka, Japan.
- [7] *BABAR* Collaboration, B. Aubert *et al.*, “A measurement of the $B^0\bar{B}^0$ oscillation frequency and determination of flavor-tagging efficiency using semileptonic and hadronic *B* decays”, *BABAR-CONF-00/08*, submitted to the XXXth International Conference on High Energy Physics, Osaka, Japan.
- [8] *BABAR* Collaboration, B. Aubert *et al.*, “A measurement of the charged and neutral *B* meson lifetimes using fully reconstructed decays”, *BABAR-CONF-00/07*, submitted to the XXXth International Conference on High Energy Physics, Osaka, Japan.
- [9] *BABAR* Collaboration, B. Aubert *et al.*, “The first year of the *BABAR* experiment at PEP-II”, *BABAR-CONF-00/17*, submitted to the XXXth International Conference on High Energy Physics, Osaka, Japan.
- [10] G. C. Fox and S. Wolfram, Phys. Rev. Lett. **41**, 1581 (1978).
- [11] Particle Data Group, D. E. Groom *et al.*, Eur. Phys. Jour. C **15**, 1 (2000).
- [12] S. Versillé, PhD Thesis (1999), Université Paris Sud-Orsay (in French).
- [13] OPAL Collaboration, K. Ackerstaff *et al.*, Eur. Phys. Jour. C **5**, 379 (1998).
- [14] CDF Collaboration, T. Affolder *et al.*, Phys. Rev. **D61**, 072005 (2000).
- [15] ALEPH Collaboration, ALEPH 99-099 CONF 99-54 (1999).